Digital camera measurements of soot temperature and soot volume fraction in axisymmetric flames

Haiqing Guo, Jose A. Castillo, and Peter B. Sunderland*

Department of Fire Protection Engineering, 3104 J.M. Patterson Building, University of Maryland, College Park, Maryland 20742, USA

*Corresponding author: pbs@umd.edu

Received 19 July 2013; revised 18 October 2013; accepted 18 October 2013; posted 21 October 2013 (Doc. ID 194228); published 15 November 2013

New diagnostics are presented that use a digital camera to measure full-field soot temperatures and soot volume fractions in axisymmetric flames. The camera is a Nikon D700 with 12 megapixels and 14 bit depth in each color plane, which was modified by removing the infrared and anti-aliasing filters. The diagnostics were calibrated with a blackbody furnace. The flame considered here was an 88 mm long ethylene/air co-flowing laminar jet diffusion flame on a round 11.1 mm burner. The resolution in the flame plane is estimated at between 0.1 and 0.7 mm. Soot temperatures were measured from soot radiative emissions, using ratio pyrometry at 450, 650, and 900 nm following deconvolution. These had a range of 1600–1850 K, a temporal resolution of 125 ms, and an estimated uncertainty of ±50 K. Soot volume fractions were measured two ways: from soot radiative emissions and from soot laser extinction at 632.8 nm, both following deconvolution. Soot volume fractions determined from emissions had a range of 0.1–10 ppm, temporal resolutions of 125 ms, and an estimated uncertainty of ±30%. Soot volume fractions determined from laser extinction had a range of 0.2–10 ppm, similar temporal resolutions, and an estimated uncertainty of ±10%. The present measurements agree with past measurements in this flame using traversing optics and probes; however, they avoid the long test times and other complications of such traditional methods.

OCIS codes: (100.1830) Deconvolution; (290.2200) Extinction; (290.6815) Thermal emission; (040.1490) Cameras.

http://dx.doi.org/10.1364/AO.52.008040

1. Introduction

Accurate measurements of soot temperature and soot concentration in flames are essential for gaining insight into many combustion processes. These measurements can be performed optically and non-intrusively in flames. Many flames of interest are axisymmetric and optically thin, which simplifies the measurements significantly.

Several studies have performed soot pyrometry following deconvolution in axisymmetric flames based on soot radiative emissions. Sunderland *et al.* [1,2] used ratio pyrometry with a photomultiplier tube at 600, 700, 750, and 830 nm, but this required traversing the optics across the flame at each height and wavelength. Gulder and co-workers [3–5] used ratio pyrometry with a spectrometer and imaged the spectra with a charge-coupled device (CCD). Again, traversing the burner horizontally at each height was required. Faeth and co-workers [6,7] used gray-scale CCD video cameras to perform ratio pyrometry (at 650 and 850 nm) in microgravity flames; however, the cameras had a low bit depth (8 bits per color plane) and a low pixel count (0.1 megapixels). Long and co-workers [8,9] used more modern color digital cameras, without external bandpass filters, for three-color ratio pyrometry. Unfortunately, the uncertainties were greater than for narrowband methods [10].

Soot volume fractions can also be found from soot radiative emissions [3,8,9,11,12], with instrument setups similar to those used in ratio pyrometry.

1559-128X/13/338040-08$15.00/0

Temperatures are determined using soot pyrometry and then these temperatures are considered with the soot radiative emissions to determine soot volume fractions. Unfortunately, the resulting uncertainties in soot volume fraction increase exponentially with uncertainties in temperature.

Soot volume fractions have also been measured in axisymmetric flames using laser extinction and assuming Rayleigh scattering from soot. Santoro *et al.* [13,14] did so in ethylene/air co-flowing diffusion flames. As with the early work in soot pyrometry, single point detectors were used, requiring extensive traversing. Full-field soot volume fraction measurements with CCD cameras were reported in [6,7,15–17]. Faeth and co-workers [6,7] used a laser diode at 632 nm; however, as in their soot pyrometry work, they used a camera with a low bit depth and a low pixel count. Gulder and co-workers [17] used a mercury arc lamp and a more advanced camera. However, arc lamps introduce unsteadiness, collimation difficulties, and uncertainties in the soot extinction coefficient.

The use of still digital cameras for combustion diagnostics is increasing [8,9,18]. As digital camera technology improves, so too do the measurements that can be performed. Recent advances in camera technology—including higher bit depth, higher pixel counts, larger sensor arrays, and decreased noise—allow nonintrusive full-field measurements in flames with increasing accuracy, speed, and spatial resolution.

This study involves the development of full-field diagnostics of soot temperature and soot volume fraction in a steady axisymmetric ethylene/air laminar diffusion flame using a digital single-lens reflex (SLR) camera. The results are compared with past measurements involving single-point detectors and thermocouples [13,14].

2. Experimental Setup

The flame considered here is an ethylene/air laminar jet diffusion flame. The burner replicates the co-flow burner of [13]. It consists of concentric brass tubes of 11.1 and 101 mm inside diameters. For the co-flow, 3 mm glass beads, followed by a 1.5 mm cell-size ceramic honeycomb, were used to obtain plug flow. The fuel tube extended 4 mm above the honeycomb. The ethylene and air flow rates were maintained at 4.35 and 856 mg/s (or 3.85 and 713 cm^3/s at laboratory conditions of 1.01 bar and 25°C). Rotameters (calibrated with soap bubble meters) were used to monitor the fuel and air flow rates. The visible flame height was 88 mm, as shown in Fig. 1(a). Measurements confirmed that the flame was steady, not soot emitting, optically thin, and axisymmetric.

A. Camera and Calibrations

A Nikon D700 color SLR camera with a 50 mm $f/1.4$ AF-D Nikkor lens was used for both soot temperature and soot volume fraction measurements. A 14 mm extension tube (Nikon PK-12) was used to obtain focus

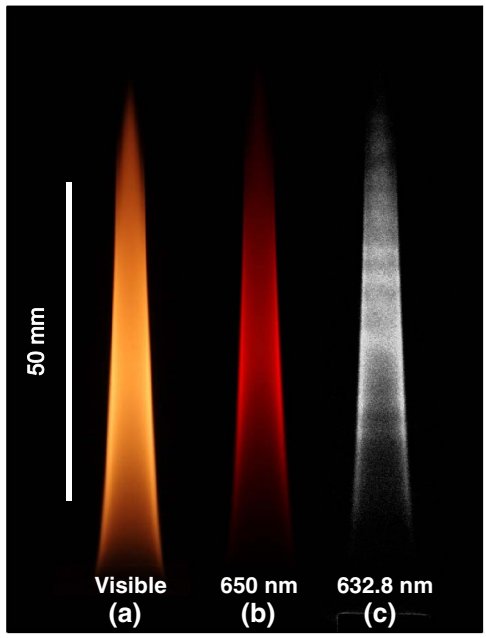

Fig. 1. Flame images: (a) color flame image, (b) color flame image with 650 nm bandpass filter, and (c) flattened laser plus flame image following subtraction of flattened laser only image.

at a distance of 24 cm from the sensor. The camera contains a 36 × 24 mm complementary metal–oxide–semiconductor (CMOS) sensor with 12 megapixels (4256 × 2832 pixels) and 14 bit depth in each of the three color planes. The camera was modified by removing the infrared cut filter, allowing measurements at 900 nm. The anti-aliasing filter was also removed to improve the focus. A long pass filter (Schott WG280) was added to maintain matched focusing at the CMOS and the eyepiece. All automatic exposure and image postprocessing options were disabled. The aperture was set to $f/4$ (for a 10 mm depth-of-field), the ISO was 200, and the white balance setting was direct sunlight. Shutter speed was optimized for each image such that no pixels were saturated in any color plane. Each image recorded the entire flame, and none of the results presented here use different images in different regions of the flame. The shutter was controlled remotely.

Images were initially saved in uncompressed Nikon-specific format. To avoid gamma corrections, the conversion to tif format was performed using Dcraw [19]. With the exceptions of "−4" and "$-T$," only default settings were used. The three color planes were flattened to grayscale using arithmetic means.

A blackbody furnace (Oriel 67032) was used to calibrate the pyrometer and to confirm linear camera response. The furnace had a 25 mm cavity opening, an emissivity of $\varepsilon = 0.99 \pm 0.01$, and a temperature accuracy of ±0.1°C. Furnace spectral radiance W_λ was obtained from Planck's law:

$$W_\lambda = \varepsilon B_\lambda = \frac{2\pi hc^2 \varepsilon}{\lambda^5 [\exp(hc/\lambda kT) - 1]}, \quad (1)$$

where B_λ is the ideal blackbody spectral radiance, c is the speed of light, h is Planck's constant, k is Boltzmann's constant, T is temperature, and λ is wavelength. For the conditions considered here the negative unity term in the denominator is negligible.

Images of the furnace at temperatures of 900°C–1200°C were recorded using the camera with each of the bandpass filters mounted to the front of the camera lens. These filters (Newport 20BPF10) were 50 mm square, had central wavelengths of 450, 650, and 900 nm, with full width at half-maximum (FWHM) bandwidths of 10 nm. The differences between the central wavelengths were much greater than the bandwidths, which simplified the pyrometry method developed below. The lens was focused on the furnace opening, which was 24 cm from the CMOS sensor. The lens focus was adjusted slightly for each wavelength to account for chromatic aberrations.

The results of these blackbody tests are summarized in Fig. 2. The abscissa here is I/ξ, where I is the irradiance incident on the CMOS sensor and is defined as

$$I = \xi \int_0^\infty \tau_\lambda W_\lambda \mathrm{d}\lambda. \tag{2}$$

Here, W_λ is from Eq. (1), τ_λ is the bandpass filter transmissivity as provided by the manufacturer, and ξ is a constant (independent of wavelength) that accounts for magnification and light losses in the lens. The integrations were performed in MATLAB. The ordinate of Fig. 2 is GS, defined as the grayscale indicated by the camera divided by the shutter time. For each filter considered, the symbols in Fig. 2 correspond to different blackbody temperatures (900°C–1200°C) and/or shutter times (0.4–20 ms). The measurements for each bandpass filter were fit according to

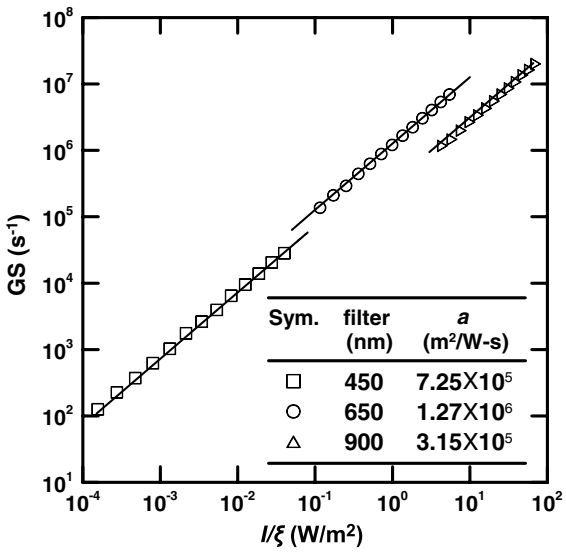

Fig. 2. Grayscale/shutter time versus irradiance incident on the sensor for each bandpass filter, as determined by blackbody measurements.

$$\mathrm{GS} = aI/\xi, \tag{3}$$

where a is a least-squares fitting constant for each filter with values given in Fig. 2. Constant a accounts for pixel size, pixel fill factor, and camera sensitivity at the wavelength of interest. The coefficient of determination (R^2) for each such fit is 0.998, or higher.

B. Soot Emission Measurements

To obtain soot temperatures and soot volume fractions from soot radiative emissions, images of the flame were recorded using the 450, 650, and 900 nm bandpass filters. Although both measurements can be performed with just two bandpass filters, this would increase the uncertainties by about 50%. Three filters yield three measurements at each point (instead of one) of both temperature and soot volume fraction. These can be used to obtain averages and to quickly identify regions where the measurements are divergent, and thus less reliable.

The camera was focused on the flame axis, which was 24 cm from the CMOS sensor. The lens focus was adjusted slightly for each wavelength to account for chromatic aberrations. Figure 1(b) shows a representative image of the flame using the 650 nm filter.

With the lens aperture set to $f/4$, all rays imaging a point in the flame onto the CMOS sensor were parallel to within ±2°. Parallel light collection was thus assumed. Smaller apertures and longer collection distances were tested to examine this assumption. These resulted in temperature differences within the experimental error, but had drawbacks of longer exposure times and decreased spatial resolution, respectively.

Each image was flattened to grayscale and, to reduce noise, grayscales were averaged vertically across 20 pixels (0.46 mm in the object plane). This level of vertical smoothing was used because temperature and soot concentration gradients are small in the vertical direction. Smoothing in the radial direction was performed using Fourier transforms with a cutoff frequency of 0.05 pixel^{-1}.

For the soot emission measurements, the pixel resolution in the object plane was 23 μm and the longest shutter time was 125 ms. Accounting for smoothing and nonparallel light in the flame plane, the vertical and radial resolution in the object plane was estimated to be 0.46 and 0.3 mm, respectively. The axis of the flame was precisely identified in each image. Because the flame was observed to be nearly axisymmetric, grayscales on both sides of the axis were averaged at each height to reduce noise.

The blackbody calibration of Eq. (3) was used to convert each measured GS to the line-of-sight integrated irradiance of soot on the CMOS sensor, I/ξ. This quantity is related to the flame properties along the line-of-sight according to [3]:

$$I(x)/\xi = \tau\Delta\lambda \int_{-\infty}^{\infty} K_{\text{abs}}(x,y) B_\lambda(x,y) \times \exp\left[-\int_y^{\infty} K_{\text{ext}}(x,y')\mathrm{d}y'\right]\mathrm{d}y, \quad (4)$$

where B_λ is defined in Eq. (1), K_{abs} and K_{ext} are the soot absorption and extinction coefficients, x (and y) are the horizontal coordinates in (and perpendicular to) the object plane, primes denote the integration variable, and τ and $\Delta\lambda$ are the peak bandpass transmissivity and FWHM, as provided by the manufacturer. Because soot primary particles (approximately 30 nm in diameter) are smaller than the Rayleigh limit (approximately 200 nm at 632.8 nm), Rayleigh scattering by soot was assumed. It is also assumed here that K_{abs} and K_{ext} are equal [3,11], such that

$$K_{\text{abs}} = 6\pi E(m) f_s/\lambda, \quad (5)$$

as used previously [1,13], where $E(m)$ is the refractive index absorption function and f_s is the soot volume fraction. Equation (5) assumes soot emissivity is proportional to λ^{-1}. Although this is the most common assumption, other studies [8,9,11,12] have proposed a soot emissivity proportional to $\lambda^{-\alpha}$, where α is a dispersion exponent between 0.95 and 1.38 and depends on wavelength and fuel type. Different values were tested here, but these resulted in temperature differences less than 50 K.

Negligible extinction of the soot radiative emissions was assumed, which yields:

$$\int_y^{\infty} K_{\text{ext}}(x,y')\mathrm{d}y' \approx 0. \quad (6)$$

This assumption was supported by the observation that the maximum extinction by the flame of any part of the 632.8 nm laser beam was 25%. For optically thick flames, corrections are required to compensate for this extinction [11,20–22]. These corrections were tested here at a few representative heights, but are not included in the results below because they resulted in temperature differences of less than 10 K. Equation (6) leads to a considerable simplification of Eq. (4).

Abel deconvolutions were performed for the 450, 650, and 900 nm images at each height, using MATLAB to convert the line-of-sight projections to radial distributions, assuming negligible extinction [23]

$$\text{GS}(r) = \mathcal{A}[\text{GS}(x)], \quad (7)$$

where $\mathcal{A}$ is the Abel deconvolution operator and r is the radius with respect to the flame axis. Note that the units returned by $\mathcal{A}$ are the units of the operand divided by length. For any pairing of bandpass filters, denoted by subscripts 1 and 2, Eqs. (3), (4), and (7) can be combined to obtain the following expression for the local soot temperature,

$$T = \frac{hc(1/\lambda_1 - 1/\lambda_2)}{k\ \ln[C_1\text{GS}_2(r)/C_2\text{GS}_1(r)]}, \quad (8)$$

where λ is the filter central wavelength and $C = a\tau\Delta\lambda/\lambda^6$ is a constant for each filter that does not vary with temperature or soot emissivity. An advantage of this ratio pyrometry is that neither $E(m)$, i.e., the soot refractive index, nor f_s appears in Eq. (8). The uncertainty in the soot temperature measurements is estimated to be ±50 K, with ±0.1 K precision for relative temperatures.

Temperatures were also measured using a thermocouple in soot-free areas. The thermocouple was an uncoated B-type thermocouple (Pt-30% Rh versus Pt-6% Rh), with a wire diameter of 51 μm and a butt-welded junction. Radiation corrections were performed as in [18], assuming a thermocouple emissivity of 0.2. Measurements were averaged over 10 s at each location. Uncertainty in the corrected thermocouple measurements is estimated to be ±40 K.

C. Soot Concentrations

Soot concentrations were measured using two independent methods. For the soot emission method, Eqs. (4), (5), and (8) are combined to obtain, for each bandpass filter,

$$f_s = \frac{\text{GS}(r)\exp(hc/k\lambda T)}{12\pi^2 hc^2 E(m) C}. \quad (9)$$

A refractive index of $m = 1.57–0.56i$ was assumed [24], which yields a refractive index absorption function of $E(m) = 0.26$. Soot refractive index varies with soot morphology, soot age, and other conditions [25,26] in a ways that are not fully understood. Other commonly invoked values of soot refractive index would change each f_s reported here by a factor of 0.9–1.25. The results of Eq. (9) are averaged for the three bandpass filters, yielding an estimated uncertainty in f_s of ±30% and a precision of $\pm 4 \times 10^{-4}$ ppm for relative soot volume fractions. The uncertainty in f_s comes mainly from the uncertainty in T, upon which f_s has the exponential dependence shown in Eq. (9).

Soot concentrations were also measured using the laser extinction system depicted in Fig. 3. The light source was a 7 mW He–Ne laser (Melles Griot 25LHR171) operating at 632.8 nm. Motivated by [16], the beam was decollimated using two diffuser

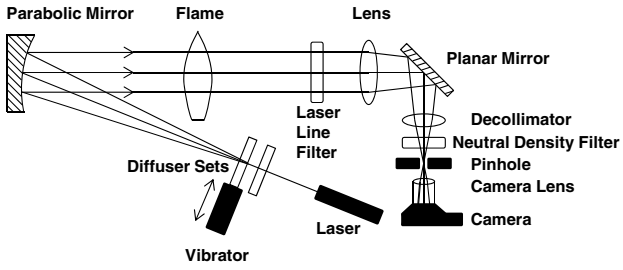

Fig. 3. Schematic of the laser extinction system.

sets (Thorlabs DG20-220 and DG20-600), the first stationary and the second mounted to a pneumatic vibrator to reduce speckle. The vibrator had an amplitude of 2.5 mm and period of 50 ms. The beam was then collimated to 100 mm using an off-axis parabolic mirror with angle of 30° and a focal length of 30 cm. After the test section, the beam passed a laser line filter at 632.8 nm with 1 nm FWHM (Andover ANDV12564) and a decollimator with a focal length of 25 cm. A neutral density filter with optical density of 2 was used to allow a shutter time of 167 ms, which is much longer than the period of the vibrator. A 3.8 mm pinhole was used to provide a 0.5° acceptance angle on the optical axis. The camera lens focus was adjusted such that, with the laser turned off, the flame plane was imaged onto the CMOS sensor.

For the laser extinction measurements, pixel resolution in the object plane was 34 μm and the shutter time was 167 ms. Accounting for smoothing and nonparallel light in the flame plane, it is estimated that the vertical and radial resolution in the flame plane was 0.68 and 0.1 mm, respectively.

Using the laser extinction system, soot volume fraction was measured for the entire flame using two images: the flame image (with the flame and the laser on) and the reference image (with the flame off and the laser on). Some past studies [16] have also recorded and subtracted images with the flame on and the laser off, but such images here had negligible grayscales owing to the 1 nm laser line filter. Figure 1(c) shows the reference image subtracted from the flame image, followed by contrast enhancement. Dim horizontal interference patterns are present as a result of the coherent light source. The negligible grayscales away from the flame arise from the good stability of the laser.

As before, shutter speed was optimized for each image, such that no pixels were saturated in any color plane; the shutter was controlled remotely; images were initially saved in uncompressed, Nikon-specific format; the conversion to tif format was performed using Dcraw [19]; the three color planes were flattened to grayscale using arithmetic means; grayscales were averaged vertically across 20 pixels (0.68 mm in the object plane); radial Fourier transforms were performed with a cutoff frequency of 0.05 pixel^{-1} for smoothing; and grayscales on both sides of the axis were averaged.

Similar to the pyrometry measurements, the flame and reference images were analyzed assuming Rayleigh scattering. Soot refractive index was again assumed to be $m = 1.57–0.56i$. The line-of-sight extinction of the incident laser by soot is

$$I(x)/I^0(x) = \exp\left(-\int_{-\infty}^{\infty} K_{\text{ext}}(x,y)\mathrm{d}y\right), \qquad (10)$$

where the superscript 0 denotes the reference image. Equation (10), combined with Eqs. (3) and (5) yields the following expression for the local soot volume fraction:

$$f_s(r) = \lambda A\{\ln[\mathrm{GS}^0(x)/\mathrm{GS}(x)]\}/6\pi E(m). \qquad (11)$$

These Abel deconvolutions were performed using MATLAB to convert the line-of-sight projections to radial distributions [23].

The uncertainty in the laser extinction soot volume fraction measurements is estimated to be ±10%, with $\pm 6 \times 10^{-4}$ ppm precision for relative soot volume fractions.

3. Results and Discussion

Full-field soot temperatures were obtained in the soot containing region with ratio pyrometry. Temperatures from the three line pairs were averaged. The difference between the average temperature and any of the three pairs was less than 30 K where soot volume fraction was above 0.5 ppm. In most regions with less than 0.5 ppm soot, noise increased and the difference between the average temperature and any of the line pairs exceeded 30 K. Therefore regions with less than 0.5 ppm soot (e.g., heights below 8 mm, and near the centerline at heights below 40 mm) are not included in the figures shown below. Note that accurate temperature measurements can be performed where the soot volume fraction is below 0.5 ppm by using longer exposures. However, longer exposures were not used here because this would have required different images in different regions of the flame.

Figure 4 shows the pyrometry results in the soot containing area at representative heights of 10, 20, 50, and 70 mm. Also shown are previous measurements of Santoro *et al.* [14], who used rapid thermocouple insertion, and the present thermocouple measurements at a height of 50 mm in the soot-free area. The pyrometry and thermocouple results obtained here are in reasonable agreement with those of Santoro *et al.* [14]. The peak temperatures in this flame are expected to be close to the adiabatic flame temperature (2370 K), but such high temperatures do not appear in Fig. 4 because there is insufficient soot to perform soot pyrometry there.

Figure 5 shows a contour plot of the soot pyrometry measurements. Temperatures were measured between 1600 and 1850 K. Temperatures outside this range exist in this flame, but are in regions with insufficient soot concentrations and/or with temperatures that are too low. Work in other flames has demonstrated the extension of this diagnostic to temperatures as low as 1000 K.

Soot volume fractions were determined from soot emissions [see Eq. (9)] using each of the 450, 650, and 900 nm bandpass filters, and then averaged. The difference between the individual determinations and the average was less than 10% at all locations. Soot volume fractions were also measured using the laser extinction system. For heights below 8 mm, insufficient soot was present for reliable measurements of the soot volume fraction.

Figure 6 shows the measured soot volume fractions at representative heights of 15 and 50 mm

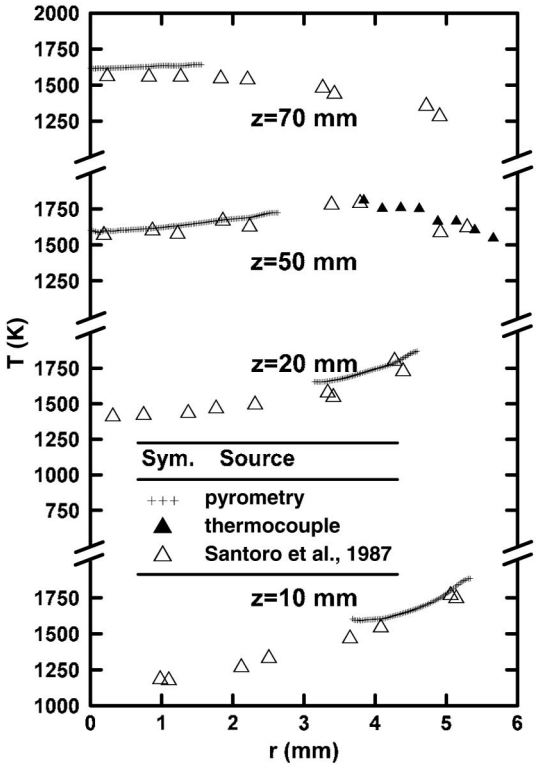

Fig. 4. Measured temperatures versus radius at heights of 10, 20, 50, and 70 mm.

above the burner for both the emission and extinction methods. Also shown are the previous measurements of Santoro *et al.* [13] using laser extinction with a point detector. The three determinations are in reasonable agreement. Small discrepancies

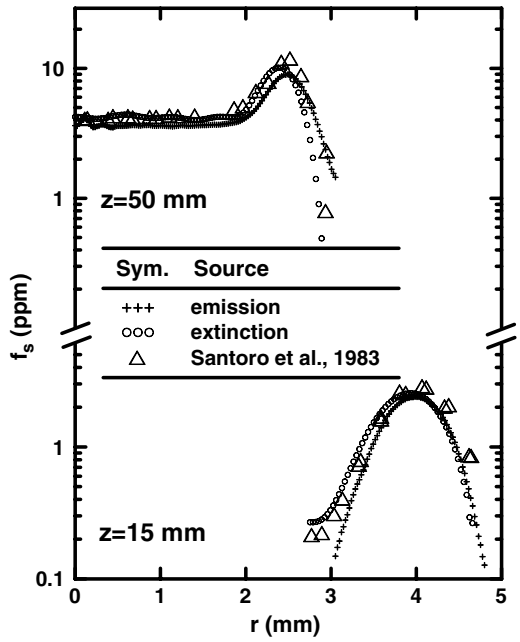

Fig. 6. Measured soot volume fractions versus radius at heights of 15 and 50 mm.

in peak soot volume fraction and location are observed, but this is within experimental uncertainties. Near the centerline at 50 mm height, radial ringing in the soot volume fraction arises owing to noise accumulation inherent in Abel deconvolutions.

Contour plots of the soot emission and the laser extinction measurements of soot volume fraction are shown in Figs. 7(a) and 7(b), respectively. The agreement between the two methods is within 15% at each

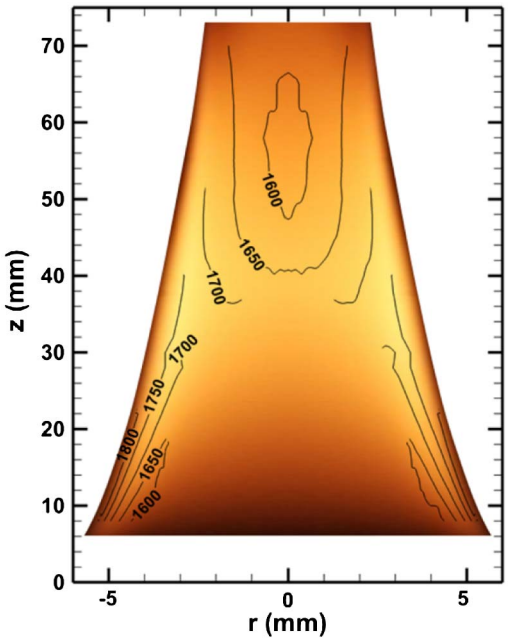

Fig. 5. Contour plot of pyrometer temperature in Kelvin, superimposed onto the color image of Fig. 1(a). The radial axis is stretched.

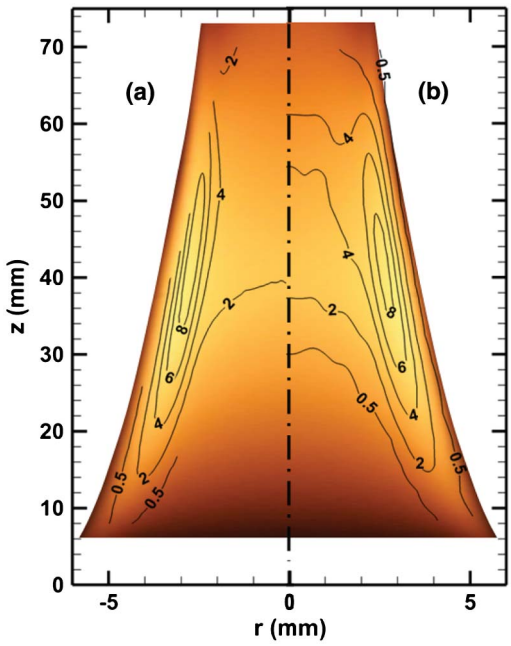

Fig. 7. Contour plots of soot volume fraction in ppm from (a) emission and (b) extinction methods, superimposed onto the color image of Fig. 1(a). The radial axis is stretched.

height. Soot volume fractions were found down to 0.1 ppm using soot emission. This limit was associated with insufficient soot concentrations and/or low temperatures. Soot volume fractions were found down to 0.2 ppm using soot extinction. This limit resulted from nonuniformities in the laser background images. Both methods were able to resolve the highest measured soot volume fractions in this flame (10 ppm). Contour plots of the temperatures and the extinction-derived soot volume fractions are shown in Fig. 8 with the flame's aspect ratio preserved.

A few comments are needed about the prospects for applying these diagnostics to different flames. First, all three methods exploited the optically thin character of the flame considered. The methods could also be applied in flames approaching optically thick conditions by accounting for self-absorption. The methods cannot be used in optically thick regions. Second, for flames with larger diameters, the measurements of both temperature and soot volume fractions would extend to lower soot volume fractions. Third, although the present flame was steady and axisymmetric, the soot extinction measurements could also be performed in unsteady axisymmetric flames that are quasi-steady on a time scale of about 125–167 ms. The other measurements could be performed in such flames by using multiple cameras or, if appropriate, by taking advantage of flame periodicity. Advanced tomographic methods with a sufficient number of cameras would allow the methods to be applied even to nonaxisymmetric flames [27].

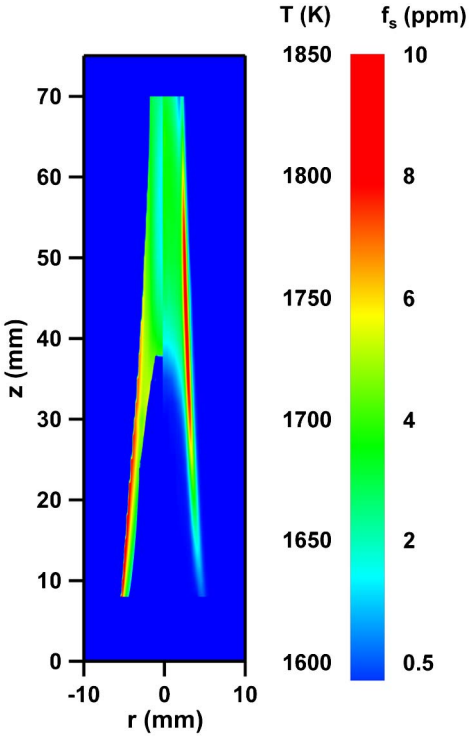

Fig. 8. Color contour plots of pyrometer temperature (left of centerline) and soot volume fraction from extinction method (right of centerline). The flame's aspect ratio is preserved.

4. Conclusions

A Nikon D700 SLR camera was used to measure soot temperature and soot volume fraction in an axisymmetric flame. The camera had CMOS sensor with a size of 36 × 24 mm, a bit depth of 14 in each color plane, and 12 megapixels. The infrared cut filter was removed to image infrared light. The flame was an 88 mm high ethylene/air coflowing laminar jet diffusion flame on an 11.1 mm burner. It was steady, soot containing, optically thin, and axisymmetric.

Soot temperatures were measured with ratio pyrometry and deconvolution. This involved filtered images at 450, 650, and 900 nm with exposures of up to 125 ms each. Temperatures were obtained between 1600 and 1850 K in the soot containing region with an estimated uncertainty of ±50 K. Soot volume fractions were measured using two methods, and both were found to agree. Using soot emissions and deconvolution at 450, 650, and 900 nm, soot volume fractions were obtained between 0.1 and 10 ppm with an estimated uncertainty of ±30%. Soot volume fractions were also measured with laser extinction at 632.8 nm and deconvolution using a camera exposure of 167 ms. Soot volume fractions were obtained between 0.2 and 10 ppm with an estimated uncertainty of ±10%. Spatial resolution in the object plane is estimated to be better than 0.7 and 0.3 mm in the vertical and radial directions, respectively. Precision was ±0.1 K for temperature and approximately $\pm 5 \times 10^4$ ppm for both determinations of soot volume fraction. The results were compared with past measurements and reasonable agreement was observed.

This work was supported by the National Science Foundation (NSF) Grant No. CBET0954441. The authors acknowledge assistance from D. L. Urban. This work was also supported by the Fulbright program under the Panama Bureau of Educational and Cultural Affairs.

References

1. P. B. Sunderland, U. O. Koylu, and G. M. Faeth, "Soot formation in weakly buoyant acetylene-fueled laminar jet diffusion flames burning in air," Combust. Flame **100**, 310–322 (1995).
2. P. B. Sunderland and G. M. Faeth, "Soot formation in hydrocarbon/air laminar jet diffusion flames," Combust. Flame **105**, 132–146 (1996).
3. D. R. Snelling, K. A. Thomson, G. J. Smallwood, O. L. Gulder, E. J. Weckman, and R. A. Fraser, "Spectrally resolved measurement of flame radiation to determine soot temperature and concentration," AIAA J. **40**, 1789–1795 (2002).
4. H. I. Joo and O. L. Gulder, "Soot formation and temperature field structure in co-flow laminar methane–air diffusion flames at pressures from 10 to 60 atm," Proc. Combust. Inst. **32**, 769–775 (2009).
5. P. M. Mandatori and O. L. Gulder, "Soot formation in laminar ethane diffusion flames at pressures from 0.2 to 3.3 MPa," Proc. Combust. Inst. **33**, 577–584 (2011).
6. D. L. Urban, Z.-G. Yuan, P. B. Sunderland, G. T. Linteris, J. E. Voss, K.-C. Lin, Z. Dai, K. Sun, and G. M. Faeth, "Structure and soot properties of nonbuoyant ethylene/air laminar jet diffusion flames," AIAA J. **36**, 1346–1360 (1998).
7. F. J. Diez, C. Aalburg, P. B. Sunderland, D. L. Urban, Z.-G. Yuan, and G. M. Faeth, "Soot properties of laminar jet diffusion flames in microgravity," Combust. Flame **156**, 1514–1524 (2009).

8. B. B. Connelly, S. A. Kaiser, M. D. Smooke, and M. B. Long, "Two-dimensional soot pyrometry with a color digital camera," *Joint Meeting of the U.S. Sections of the Combustion Institute*, Philadelphia, Pennsylvania, USA, March 2005.
9. P. B. Kuhn, B. Ma, B. C. Connelly, M. D. Smooke, and M. B. Long, "Soot and thin-filament pyrometry using a color digital camera," Proc. Combust. Inst. **33**, 743–750 (2011).
10. T. Fu, X. Cheng, and Z. Yang, "Theoretical evaluation of measurement uncertainties of two-color pyrometry applied to optical diagnostics," Appl. Opt. **47**, 6112–6123 (2008).
11. S. D. Iuliis, M. Barbini, S. Benecchi, F. Cignoli, and G. Zizak, "Determination of the soot volume fraction in an ethylene diffusion flame by multiwavelength analysis of soot radiation," Combust. Flame **115**, 253–261 (1998).
12. Y. Matsui, T. Kamimoto, and S. Matsuoka, "A study on the time and space resolved measurement of flame temperature and soot concentration in a D.I. diesel engine by the two-color method," SAE Technical Paper 790491, 1808–1822, (1979).
13. R. J. Santoro, H. G. Semerjian, and R. A. Dobbins, "Soot particle measurements in diffusion flames," Combust. Flame **51**, 203–218 (1983).
14. R. J. Santoro, T. T. Yeh, J. J. Horvath, and H. G. Semerjian, "The transport and growth of soot particles in laminar diffusion flames," Combust. Sci. Technol. **53**, 89–115 (1987).
15. P. S. Greenberg and J. C. Ku, "Soot volume fraction imaging," Appl. Opt. **36**, 5514–5522 (1997).
16. C. P. Arana, M. Pontoni, S. Sen, and I. K. Puri, "Field measurements of soot volume fractions in laminar partially premixed coflow ethylene/air flames," Combust. Flame **138**, 362–372 (2004).
17. D. R. Snelling, K. A. Thomson, G. J. Smallwood, and O. L. Gulder, "Two-dimensional imaging of soot volume fraction in laminar diffusion flames," Appl. Opt. **38**, 2478–2485 (1999).
18. J. D. Maun, P. B. Sunderland, and D. L. Urban, "Thin-filament pyrometry with a digital still camera," Appl. Opt. **46**, 483–488 (2007).
19. D. Coffin, "Decoding raw digital photos in Linux," http://www.cybercom.net/~dcoffin/dcraw/.
20. P. Elder, T. Jerrick, and J. W. Birkeland, "Determination of the radial profile of absorption and emission coefficients and temperature in cylindrically symmetric sources with self-absorption," Appl. Opt. **4**, 589–592 (1965).
21. S. J. Young, "Iterative Abel inversion of optically thick, cylindrically symmetric radiation sources," J. Quant. Spectrosc. Radiat. Transfer **25**, 479–481 (1981).
22. Y. Wang, P. Ding, and Y. Mu, "A spline approximation of the Abel transformation for use in optically-thick, cylindrically-symmetric plasmas," J. Quant. Spectrosc. Radiat. Transfer **54**, 1055–1058 (1995).
23. Z.-G. Yuan, "The filtered Abel transform and its application in combustion diagnostics," *Western States Section of the Combustion Institute*, Stanford, CA, USA, October, 1995.
24. W. H. Dalzell, G. C. Williams, and H. C. Hottel, "A light-scattering method for concentration measurements," Combust. Flame **14**, 161–169 (1970).
25. K. C. Smyth and C. R. Shaddix, "Brief communication: the elusive history of m=1.57–0.56i for the refractive index of soot," Combust. Flame **107**, 314–320 (1996).
26. S. C. Lee and C. L. Tien, "Optical constants of soot in hydrocarbon flames," Symp. (Int.) Combust., [Proc.] **18**, 1159–1166 (1981).
27. D. Liu, Q. X. Huang, F. Wang, Y. Chi, K. F. Cen, and Y. H. Yan, "Simultaneous measurement of three-dimensional soot temperature and volume fraction fields in axisymmetric or asymmetric small unconfined flames with CCD Cameras," Trans. ASME **132**, 061202 (2010).